micromachines

Article

Thermal Management of Serpentine Flexible Heater Based on the Orthotropic Heat Conduction Model

Zhao Zhao [1], Jin Nan [2] and Min Li [1,3,*]

[1] Institute of Solid Mechanics, Beihang University (BUAA), Beijing 100191, China; ouczhaozhao@163.com
[2] School of Mechanics and Civil Engineering, China University of Mining and Technology, Beijing 100083, China; nanjincn@163.com
[3] Aircraft and Propulsion Laboratory, Ningbo Institute of Technology, Beihang University (BUAA), Ningbo 315100, China
* Correspondence: limin@buaa.edu.cn

Abstract: Flexible heaters can perfectly fit with undevelopable surfaces for heating in many practical applications such as thermotherapy, defogging/deicing systems and warming garments. Considering the requirement for stretchability in a flexible heater, certain spacing needs to be retained between serpentine heat sources for deformation which will inevitably bring critical challenges to the thermal uniformity. In order to reconcile these two conflicting aspects, a novel method is proposed by embedding the serpentine heat source in orthotropic layers to achieve comprehensive performance in stretchability and uniform heating. Such a scheme takes advantage of the ability of orthotropic material to control the heat flow distribution via orthotropic thermal conductivity. In this paper, an analytical heat conduction model with orthotropic substrate and encapsulation is calculated using Fourier cosine transform, which is validated by finite element analysis (FEA). Meanwhile, the effects of the orthotropic substrate or encapsulation with different ratios of thermal conductivity and the geometric spacing on the thermal properties are investigated, which can help guide the design and fabrication of flexible heaters to achieve the goal of uniform heating.

Keywords: orthotropic heat conduction; flexible heater; serpentine heat source; thermal uniformity

Citation: Zhao, Z.; Nan, J.; Li, M. Thermal Management of Serpentine Flexible Heater Based on the Orthotropic Heat Conduction Model. *Micromachines* **2022**, *13*, 622. https://doi.org/10.3390/mi13040622

Academic Editor: Rui Li

Received: 15 March 2022
Accepted: 13 April 2022
Published: 15 April 2022

1. Introduction

A flexible heater, as a novel heating device, is widely used in heating undevelopable curved surfaces, such as in cutaneous wound healing [1], subcutaneous tumor treatment [2], thermal releasing drug [3], defogging/deicing systems [4,5], heatable curved windows [6] and so on.

Recently, there has been a variety of advancements in developing flexible heaters based on stretchable polymers with conductive compositions [7]. For example, a metal nano network [8], copper-plated fibers [9] and graphite [10] as flexible heaters have been investigated. However, the slippage of fiber in these heaters will result in higher electrical resistance in the local position under deformation, which causes extraordinarily higher temperatures at this point (i.e., called "hot spots") [9]. To avoid this problem, periodical metal wire as a heat source was developed in flexible heaters. Jang [11] investigated a stretchable and uniform Kirigami heater for heating the wrist and elbow with large motions, where aluminum-doped conductive paper is processed into a stretchable shape. Chen et al. [12] adopted a copper mesh heat source as a skin patch for thermotherapy, which was shown to be highly conformable to the skin at high stretching.

On the other hand, a stretchable design for heat sources requires certain spacing to keep deformability, which will result in uneven temperatures at these positions. In order to keep balance with better mechanical compatibility and temperature uniformity, a heat source is designed with a serpentine structure [13–15] embedded in orthotropic substrate and encapsulation. Significantly, the orthotropic model based on a multilayered composite

material (i.e., thermal metamaterials) can control the temperature and the manipulation of thermal flux via thermal anisotropy [16–18]; it can help achieve the goal of temperature uniformity. As for thermal management in flexible electronics, many analytical heat conduction models have been investigated in previous studies. For example, a heat conduction model of a single and an infinite number of rectangular heat sources in an isotropic model was developed [19,20] based on the transfer matrix method and Fourier heat transfer. Additionally, the Hankel transform was used to solve the heat conduction of a point heat source in flexible electronic devices [21].

Compared to the regular heat sources in previous studies, the analytical orthotropic heat conduction model with the complex serpentine heat source is developed in this paper. The thermal field of the model is calculated using Fourier cosine transform and linear superposition of a rectangular heat source in Section 2, which is validated by Finite element analysis (FEA) in Section 3. Meanwhile, the effects of different ratios of thermal conductivity in substrate/encapsulation and different spacing of the serpentine heat source on the thermal properties are discussed. Section 4 presents the conclusion.

2. Analytical Modeling

Figure 1a shows the flexible heater with periodic serpentine heat sources embedded in the orthotropic substrate and encapsulation. Due to periodicity, only a unit cell is investigated, as shown in Figure 1b.

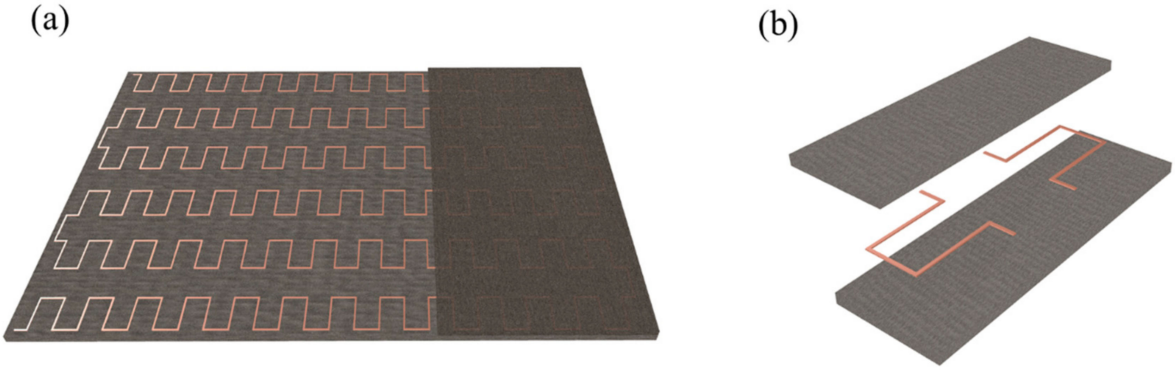

Figure 1. (**a**) Schematic diagram of serpentine heat source embedded in orthotropic membranes; (**b**) a single period of the periodic structure.

As for thermal properties in the orthotropic model, the thermal conductivities in layered thermal metamaterials consist of two kinds of material yield, [16,22]

$$k^m = \frac{k_A + k_B}{2}, k^n = \frac{2k_A k_B}{k_A + k_B} \quad (1)$$

where k^m and k^n are the thermal conductivity along in-plane and off-plane (i.e., the laying direction of different materials) directions, respectively. K_A and k_B represent the thermal conductivity of layered materials A and B. The geometric parameters of a period of serpentine heat source, including the vertical space W_1, the horizontal space W_2, the width t and the length of straight part l, are shown in Figure 2a. Due to symmetry, only a quarter of the heat conduction model consisting of encapsulation, substrate and the heat source is studied in Figure 2b. Compared with the whole thickness of the model, the ultrathin serpentine heat source (thickness of copper selected as 2.6 μm [23]) based on micro-nano machining is negligible in this paper, which can be regarded as a planar heat source in heat conduction [24].

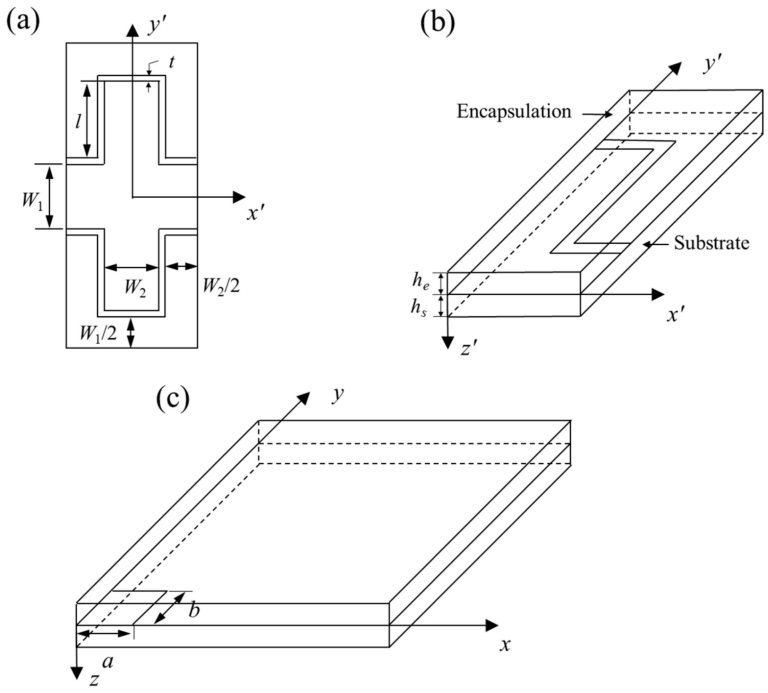

Figure 2. Schematic diagrams of (**a**) a single period and (**b**) a quarter of the model; (**c**) a rectangle heat source embedded in a quarter of the model with infinite size in the plane.

In this paper, the temperature increase in the infinite plane model with any arbitrary size of a rectangular planar heat source is calculated at first (shown in Figure 2c), then the linear superposition principle is used to obtain the temperature increase distribution of the serpentine structure in the unit cell. Figure 2c presents a quarter of the model with infinite size in the plane, where the coordinate system is established at the center of the rectangle planar heat source as the origin, the x-axis and y-axis follow the a and b sides, respectively, and the z-axis points from the heat source to the substrate. The temperature in the system is denoted by $T_{\mathrm{i}}(x,y,z)$, and thus, the temperature increase in the model is denoted by $\theta_i = T_i - T_\infty$ from the ambient temperature T_∞. The heat conduction equation in the orthotropic model gives

$$k_i^x \frac{\partial^2 \theta_i}{\partial x^2} + k_i^y \frac{\partial^2 \theta_i}{\partial y^2} + k_i^z \frac{\partial^2 \theta_i}{\partial z^2} = 0 \tag{2}$$

where i can be e (encapsulation) and s (substrate). k^x, k^y and k^z denote the thermal conductivity in the x, y and z-direction, respectively. At the top and bottom surfaces of the structure, the natural convection condition yields

$$-k_s^z \frac{\partial \theta_s}{\partial z}\bigg|_{z=h_s} = h_0 \theta_s \tag{3}$$

$$k_e^z \frac{\partial \theta_e}{\partial z}\bigg|_{z=-h_e} = h_0 \theta_e \tag{4}$$

where h_0 is the coefficient of heat convection. Considering the continuity of temperature increase and heat flux on the interface with the heat source between the substrate and encapsulation, it can be expressed by

$$\theta_e|_{z=0^-} = \theta_s|_{z=0^+} \tag{5}$$

$$k_e^z \frac{\partial \theta_e}{\partial z}\bigg|_{0^-} - k_s^z \frac{\partial \theta_s}{\partial z}\bigg|_{0^+} = \begin{cases} Q_0, \ (x,y) \in D \\ 0, (x,y) \notin D \end{cases} \tag{6}$$

where D and Q_0 are the region and the heat flux density of the rectangle planar heat source. Using the Fourier cosine transform, the temperature increase in the model can be written as

$$\overline{\theta_i}(\alpha,\beta,z) = \int_0^\infty \int_0^\infty \theta_i(x,y,z)\cos(\alpha x)\cos(\beta y)\mathrm{d}x\mathrm{d}y \tag{7}$$

which is used to solve the definite solutions of steady heat conduction in the model. Therefore, Equations (2)–(6) based on the Fourier cosine transform become

$$\frac{\mathrm{d}^2\overline{\theta_i}}{\mathrm{d}z^2} - \left(\frac{\alpha^2 k_i^x + \beta^2 k_i^y}{k_i^z}\right)\overline{\theta_i} = 0 \tag{8}$$

$$-k_s^z \frac{\mathrm{d}\overline{\theta_s}}{\mathrm{d}z}\bigg|_{z=h_s} = h_0 \overline{\theta_s} \tag{9}$$

$$k_e^z \frac{\mathrm{d}\overline{\theta_e}}{\mathrm{d}z}\bigg|_{z=-h_e} = h_0 \overline{\theta_e} \tag{10}$$

$$\overline{\theta_e}\big|_{z=0^-} = \overline{\theta_s}\big|_{z=0^+} \tag{11}$$

$$k_e^z \frac{\mathrm{d}\theta_e}{\mathrm{d}z}\bigg|_{0^-} - k_s^z \frac{\mathrm{d}\theta_s}{\mathrm{d}z}\bigg|_{0^+} = \frac{Q_0 \sin(\alpha a)\sin(\beta b)}{\alpha\beta} \tag{12}$$

The general solution in Equation (8) can be expressed by

$$\overline{\theta_i} = A_i e^{\sqrt{\frac{\alpha^2 k_i^x + \beta^2 k_i^y}{k_i^z}}z} + B_i e^{-\sqrt{\frac{\alpha^2 k_i^x + \beta^2 k_i^y}{k_i^z}}z} \tag{13}$$

The coefficients A_s, A_e, B_s and B_e in Equation (13) are determined by Equations (9)–(12), which can be obtained by

$$\begin{aligned}
A_s &= \frac{1}{\alpha\beta}\frac{\sin(a\alpha)\sin(b\beta)(h_0-C_1)\left((h_0-C_2)e^{-2h_e\xi_e}-C_2-h_0\right)Q_0}{\left[\begin{array}{c}\Big((C_1-C_2)(h_0+C_1)e^{2h_s\xi_s}+(C_1+C_2)(h_0-C_1)\Big)(C_2-h_0)e^{-2h_e\xi_e} \\ +\Big((C_1+C_2)(h_0+C_1)e^{2h_s\xi_s}+(C_1-C_2)(h_0-C_1)\Big)(h_0+C_2)\end{array}\right]}, \\
A_e &= \frac{1}{\alpha\beta}\frac{\sin(a\alpha)\sin(b\beta)(h_0+C_2)\left((h_0+C_1)e^{2h_s\xi_s}+C_1-h_0\right)Q_0}{\left[\begin{array}{c}\Big((C_1+C_2)(h_0+C_2)-(C_1-C_2)(h_0-C_2)e^{-2h_e\xi_e}\Big)(h_0+C_1)e^{2h_s\xi_s} \\ -\Big((C_1+C_2)(h_0-C_2)e^{-2h_e\xi_e}-(C_1-C_2)(h_0+C_2)\Big)(h_0-C_1)\end{array}\right]}, \\
B_s &= -\frac{A_s(h_0+C_1)e^{2h_s\xi_s}}{h_0-C_1}, \\
B_e &= -\frac{A_e(h_0-C_2)e^{-2h_e\xi_e}}{h_0+C_2}
\end{aligned} \tag{14}$$

where

$$\xi_i = \sqrt{\frac{\alpha^2 k_i^x + \beta^2 k_i^y}{k_i^z}}, \ C_1 = \xi_s k_s^z, \ C_2 = \xi_e k_e^z \tag{15}$$

So far, the temperature increase in the model can be calculated based on inverse Fourier cosine transform, which gives

$$\theta_i(x,y,z) = \frac{4}{\pi^2}\int_0^\infty \int_0^\infty \overline{\theta_i}(\alpha,\beta,z)\cos(\alpha x)\cos(\beta y)\mathrm{d}\alpha\mathrm{d}\beta \tag{16}$$

The serpentine heat source shown in Figure 1a can be divided into many rectangular heat sources. According to the relative coordinates (x_j, y_j) of the geometric center point

of each rectangular heat source in the x'-y'-z' coordinate system shown in Figure 2b, the temperature increase in a unit cell can be obtained through linear superposition of the surrounding heat source, which can be written as

$$\theta_i(x,y,z) = \frac{4}{\pi^2}\sum_{j=1}^{\infty}\int_0^{\infty}\int_0^{\infty}\overline{\theta_i}(\alpha,\beta,z)\cos\left(\alpha\left(x-x_j\right)\right)\cos\left(\beta\left(y-y_j\right)\right)\mathrm{d}\alpha\mathrm{d}\beta \quad (17)$$

3. Results and Discussion

In this section, the orthotropic heat conduction model with the serpentine heat source is verified by FEA. Additionally, the effects of geometric spacing and the orthotropic thermal conductivity on the thermal properties are investigated. The encapsulation is selected as polyurethane (PU) with the thermal conductivity 0.19 W/m/K [25], and PDMS is used as substrate with the thermal conductivity 0.17 W/m/K [26]. The natural air convection coefficient h_0 on the top and bottom surfaces is 15 W/m^2/K. The power density is set as Q_0 = 10 mW/mm^2. As for the geometric parameters of the structure, they are selected as: the vertical space W_1 = 5 mm, the horizontal space W_2 = 3 mm, the width t = 0.2 mm, the length of straight part l = 5 mm and the thickness of substrate and encapsulation $h_e = h_s$ = 1 mm. In FEA, 2.5 million DC3D8 heat transfer elements are dispersed in the ABAQUS software and obtain the convergence result.

As a wearable heater in the future, the temperature distribution on the bottom surface of the substrate is noteworthy because it is in contact with the target object, such as the skin. Figure 3 shows the thermal fields at the bottom surface in a quarter of the unit cell (as shown in Figure 2b), which are calculated using Equation (17) based on the linear superposition of the surrounding heat source. Figure 3a shows the comparison of the temperature field between the analytical and FEA in a quarter of the unit isotropic cell with $k_s{}^x = k_s{}^y = k_s{}^z$ = 0.17 W/m/K in the substrate. It can be seen that the temperature distribution is uneven along the y-direction because of the larger spacing W_1 between serpentine heat sources. In general, the designed vertical space W_1 is larger than the horizontal space W_2 if the stretchable design of structure is along the horizontal direction (Figure 1), because most of the structures will shrink along the vertical direction based on the positive Poisson's effect under horizontal stretching. To improve the temperature uniformity, the $k_s{}^y$ is set as 1.7 W/m/K and other parameters are fixed, which is based on the different materials in the substrate laying along the y-direction (i.e., off-plane direction) in Equation (1). Figure 3b illustrates that the orthotropic substrate with higher $k_s{}^y$ has a positive influence on the temperature uniformity, which is validated by FEA.

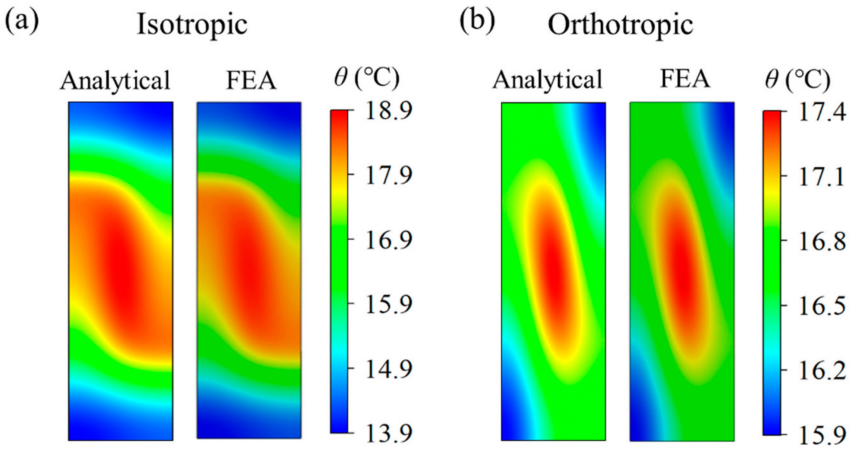

Figure 3. Comparison of the analytical and FEA temperature field on the bottom surface of a quarter of the unit cell based on (**a**) the isotropic and (**b**) orthotropic substrate.

In order to show more direct comparison results, the temperature distributions along the different paths on the bottom surface of a quarter of the unit cell based on the isotropic and orthotropic substrate are shown in Figure 4. The temperature increase on the line starting from the coordinate origin (0, 0) to the coordinate (3.2, 10.4) of the upper right corner of a quarter model is calculated in Figure 4a, which includes the maximum and the minimum temperature in the model. It can be observed that the orthotropic substrate with higher $k_s{}^y$ effectively reduces the temperature difference. From Figure 4b, the temperature difference between the isotropic and orthotropic substrates is close along the x direction (y = 2.5 mm); nevertheless, there is a great difference along the y-direction (x = 0), as shown in Figure 4c. This is because the higher thermal conductivity $k_s{}^y$ in the y-direction can help obtain the uniform temperature distribution along the vertical space W_1.

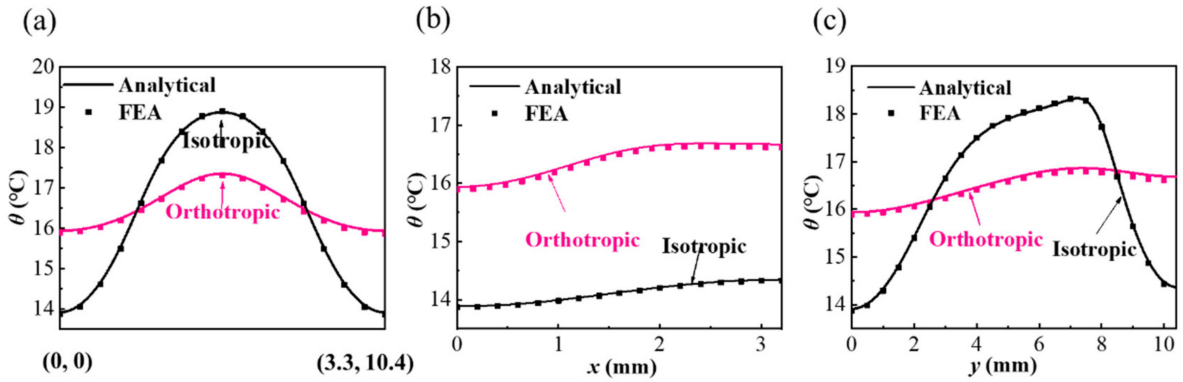

Figure 4. The comparisons of temperature increase along (**a**) the line from (0, 0) to (3.2, 10.4), (**b**) y = 2.5 and (**c**) x = 0 on the bottom surface a quarter of unit cell between the analytical results and FEA.

The variable thermal conductivity in different directions of the substrate can be used for thermal management in different purposes via changing the laying direction of materials. For example, a better uniform temperature distribution can be achieved with the increased thermal conductivity ratio of $k_s{}^y/k_s{}^x$, as shown in Figure 5a, but there is an opposite trend with increasing $k_s{}^z/k_s{}^x$ in Figure 5b. The increasing $k_s{}^z$ means the heat conduction increases along the z-direction more quickly, thus reducing the in-plane heat diffusion, which has a negative effect on the uniform temperature on the bottom surface of the substrate.

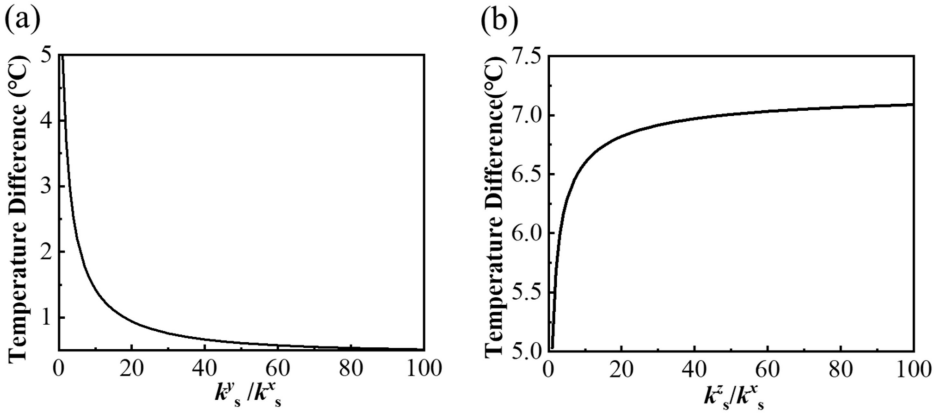

Figure 5. Effects of the orthotropic substrate with different ratios of (**a**) $k_s{}^y/k_s{}^x$ and (**b**) $k_s{}^z/k_s{}^x$ on the thermal uniformity of the bottom surface of the model.

Figure 6 illustrates geometric effects of vertical space W_1 and horizontal space W_2 on the thermal properties of models with isotropic ($k_s{}^x = k_s{}^y = k_s{}^z$ = 0.17 W/m/K) and or-

thotropic substrate ($k_s{}^x = k_s{}^z = 0.17$ W/m/K and $k_s{}^y = 1.7$ W/m/K). It can be observed from Figure 6a,b that the maximum (T_{max}) and the minimum (T_{min}) temperature decreases with the increasing spaces. Figure 6c shows that the temperature difference in the orthotropic model is lower than that in the isotropic model with different W_1, which is the same as models with different W_2 shown in Figure 6d. The result shows that the orthotropic substrate with larger $k_s{}^y$ can help improve the temperature uniformity on the bottom surface with different spaces, W_1 and W_2, of heat sources. When the W_1 is increasing, the temperature uniformity of the orthotropic model is better than the isotropic model, as shown in Figure 6c. Meanwhile, there is an interesting trend in the isotropic model shown in Figure 6d that the temperature difference is not monotonic with the increasing W_2, because the T_{max} drops faster than T_{min} in the isotropic model in the certain area of W_2.

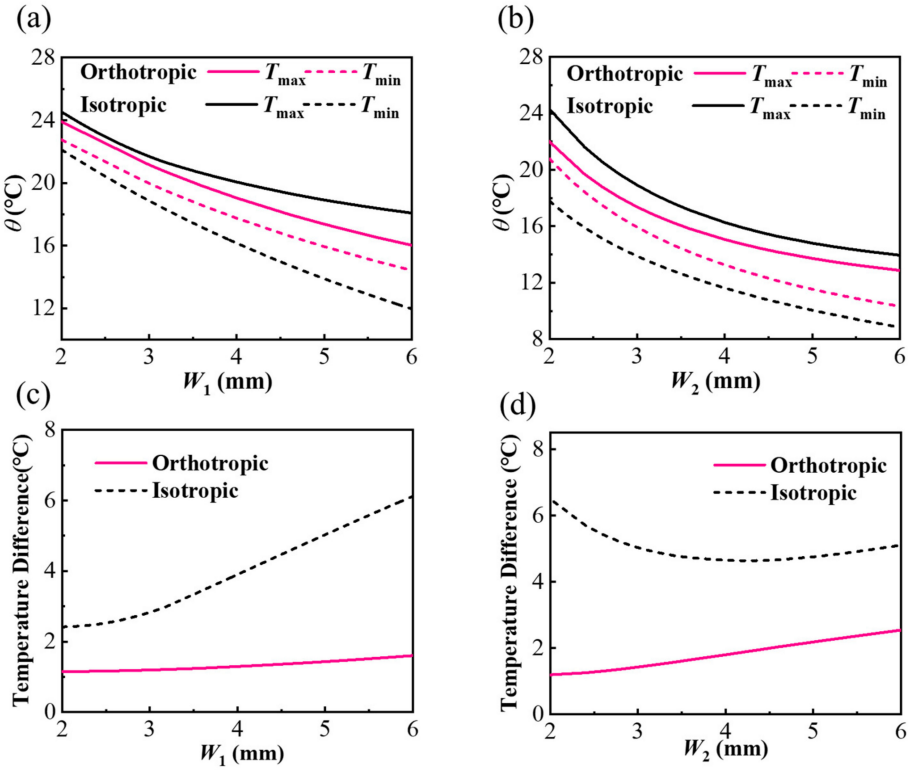

Figure 6. (**a**,**b**) The maximum (T_{max}), the minimum (T_{min}) temperature and (**c**,**d**) temperature difference on the bottom surface of the orthotropic and isotropic model with different vertical space W_1 and horizontal space W_2.

The above research mainly focuses on the orthotropic substrate. In fact, the temperature distribution on the bottom surface of the substrate also depends on the thermal characteristics of the encapsulation. Therefore, the orthotropic encapsulation with different thermal conductivity ratios of $k_e{}^y/k_e{}^x$ and $k_e{}^z/k_e{}^x$ are investigated in Figure 7, where the substrate is selected as the isotropic substrate. It can be seen that the temperature difference decreases with the increasing $k_e{}^y/k_e{}^x$ and $k_e{}^z/k_e{}^x$, because the improvement of the thermal conductivity of the encapsulation can effectively transfer heat to the top layer, thus reducing the heat flow in the substrate, which can help improve the uniform temperature of the bottom surface on the substrate. Additionally, the thermal conductivity $k_e{}^z$ in encapsulation has a greater impact on the temperature uniformity on the bottom surface because the temperature difference falls faster than that with $k_e{}^y$, as shown in Figure 7.

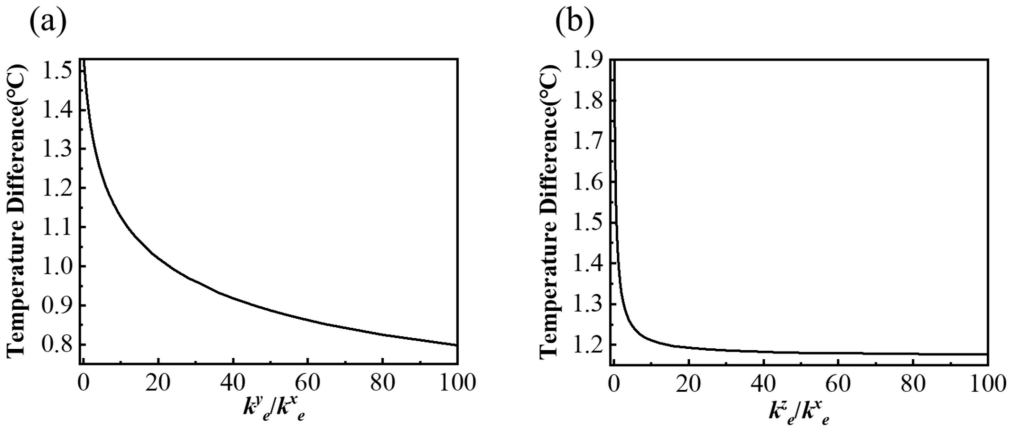

Figure 7. Effects of the orthotropic encapsulation with different ratios of (**a**) $k_e{}^y/k_e{}^x$ and (**b**) $k_e{}^z/k_e{}^x$ on the thermal uniformity of the bottom surface of the model.

4. Conclusions

In summary, this paper presents an analytical orthotropic heat conduction model with a serpentine heat source, which is validated by FEA. Unlike traditional heating components with a regular heat source shape and isotropic materials, the orthotropic flexible heater is used for uniform heating via adjusting the thermal conductivity in different directions. The temperature distribution on the bottom surface of the model is taken as the research object, which is the surface in contact with the target object. The results show that the higher thermal conductivity of substrate $k_s{}^y$ along the vertical spacing of the heat source can effectively improve the temperature uniformity with different geometric spacing. On the contrary, improving the thermal conductivities of the substrate along other directions is ineffective. Additionally, the higher thermal conductivity of orthotropic encapsulation can obtain thermal uniformity as well. This study can be exploited in the design of a serpentine heater with the orthotropic model and provide easily interpretable guidelines to control the temperature distribution.

Author Contributions: Conceptualization, M.L.; methodology, Z.Z.; software, J.N.; validation, Z.Z., J.N. and M.L.; formal analysis, Z.Z.; investigation, Z.Z. and J.N.; resources, M.L.; data curation, Z.Z. and J.N.; writing—original draft preparation, Z.Z.; writing—review and editing, M.L.; visualization, Z.Z.; supervision, M.L.; project administration, M.L.; funding acquisition, M.L. All authors have read and agreed to the published version of the manuscript.

Funding: This research was funded by the Natural Science Foundation of Zhejiang Province of China (Grant number LY21A020001), and Ningbo Scientific and Technological Innovation 2025 Major Project (Grant number 2021Z108).

Acknowledgments: The Natural Science Foundation of Zhejiang Province of China (No. LY21A020001) and Ningbo Scientific and Technological Innovation 2025 Major Project (No. 2021Z108).

Conflicts of Interest: The authors declare no conflict of interest.

References

1. Hattori, Y.; Falgout, L.; Lee, W.; Jung, S.Y.; Poon, E.; Lee, J.W.; Na, I.; Geisler, A.; Sadhwani, D.; Zhang, Y. Multifunctional skin-like electronics for quantitative, clinical monitoring of cutaneous wound healing. *Adv. Healthc. Mater.* **2014**, *3*, 1597–1607. [CrossRef] [PubMed]
2. Wang, Q.; Sheng, H.; Lv, Y.; Liang, J.; Liu, Y.; Li, N.; Xie, E.; Su, Q.; Ershad, F.; Lan, W. A Skin-Mountable Hyperthermia Patch Based on Metal Nanofiber Network with High Transparency and Low Resistivity toward Subcutaneous Tumor Treatment. *Adv. Funct. Mater.* **2022**, 2111228. [CrossRef]
3. Tamayol, A.; Hassani, N.A.; Mostafalu, P.; Yetisen, A.K.; Commotto, M.; Aldhahri, M.; Abdel-Wahab, M.S.; Najafabadi, Z.I.; Latifi, S.; Akbari, M. Biodegradable elastic nanofibrous platforms with integrated flexible heaters for on-demand drug delivery. *Sci. Rep.* **2017**, *7*, 1–10.

4. Hong, S.; Lee, H.; Lee, J.; Kwon, J.; Han, S.; Suh, Y.D.; Cho, H.; Shin, J.; Yeo, J.; Ko, S.H. Highly Stretchable and Transparent Metal Nanowire Heater for Wearable Electronics Applications. *Adv. Mater.* **2015**, *27*, 4744–4751. [CrossRef] [PubMed]
5. Roy, R.; Raj, L.P.; Jo, J.H.; Cho, M.Y.; Kweon, J.H.; Myong, R.S. Multiphysics anti-icing simulation of a CFRP composite wing structure embedded with thin etched-foil electrothermal heating films in glaze ice conditions. *Compos Struct.* **2021**, *276*, 114441. [CrossRef]
6. Kamalisarvestani, M.; Saidur, R.; Mekhilef, S.; Javadi, F.S. Performance materials and coating technologies of thermochromic thin films on smart windows. *Renew. Sustain. Energy Rev.* **2013**, *26*, 353–364. [CrossRef]
7. Kim, D.C.; Shim, H.J.; Lee, W.; Koo, J.H.; Kim, D.H. Material-Based Approaches for the Fabrication of Stretchable Electronics. *Adv. Mater.* **2020**, *32*, 1902743. [CrossRef]
8. An, B.W.; Gwak, E.J.; Kim, K.; Kim, Y.C.; Jang, J.; Kim, J.Y.; Park, J.U. Stretchable, Transparent Electrodes as Wearable Heaters Using Nanotrough Networks of Metallic Glasses with Superior Mechanical Properties and Thermal Stability. *Nano Lett.* **2016**, *16*, 471–478. [CrossRef]
9. Jo, H.S.; An, S.; Lee, J.G.; Park, H.G.; Al-Deyab, S.S.; Yarin, A.L.; Yoon, S.S. Highly flexible, stretchable, patternable, transparent copper fiber heater on a complex 3D surface. NPG. *Asia Mater.* **2017**, *9*, e347. [CrossRef]
10. Bilodeau, R.A.; Nasab, A.M.; Shah, D.S.; Kramer-Bottiglio, R. Uniform conductivity in stretchable silicones via multiphase inclusions. *Soft Matter* **2020**, *16*, 5827–5839. [CrossRef]
11. Jang, N.S.; Kim, K.H.; Ha, S.H.; Jung, S.H.; Lee, H.M.; Kim, J.M. Simple approach to high-performance stretchable heaters based on kirigami patterning of conductive paper for wearable thermotherapy applications. *ACS Appl. Mater. Interfaces* **2017**, *9*, 19612–19621. [CrossRef]
12. Chen, X.L.; Yin, Y.F.; Yuan, W.; Nie, S.H.; Lin, Y.; Guo, W.R.; Su, W.M.; Li, Y.H.; Yang, K.; Cui, Z. Transparent Thermotherapeutic Skin Patch Based on Highly Conductive and Stretchable Copper Mesh Heater. *Adv. Electron. Mater.* **2021**, *7*, 2100611. [CrossRef]
13. Fan, Z.C.; Zhang, Y.H.; Ma, Q.; Zhang, F.; Fu, H.R.; Hwang, K.C.; Huang, Y.G. A finite deformation model of planar serpentine interconnects for stretchable electronics. *Int. J. Solids Struct.* **2016**, *91*, 46–54. [CrossRef]
14. Li, K.; Cheng, X.; Zhu, F.; Li, L.; Xie, Z.Q.; Luan, H.W.; Wang, Z.H.; Ji, Z.Y.; Wang, H.L.; Liu, F.; et al. A Generic Soft Encapsulation Strategy for Stretchable Electronics. *Adv. Funct. Mater.* **2019**, *29*, 1806630. [CrossRef]
15. Nie, S.; Cai, M.; Wang, C.J.; Song, J.Z. Fatigue Life Prediction of Serpentine Interconnects on Soft Elastomers for Stretchable Electronics. *J. Appl. Mech.* **2020**, *87*, 011011. [CrossRef]
16. Vemuri, K.P.; Bandaru, P.R. Geometrical considerations in the control and manipulation of conductive heat flux in multilayered thermal metamaterials. *Appl. Phys. Lett.* **2013**, *103*, 133111. [CrossRef]
17. Vemuri, K.P.; Bandaru, P.R. Anomalous refraction of heat flux in thermal metamaterials. *Appl. Phys. Lett.* **2014**, *104*, 083901. [CrossRef]
18. Yang, T.; Vemuri, K.P.; Bandaru, P.R. Experimental evidence for the bending of heat flux in a thermal metamaterial. *Appl. Phys. Lett.* **2014**, *105*, 083908. [CrossRef]
19. Cui, Y.; Li, Y.H.; Xing, Y.F.; Yang, T.Z.; Song, J.Z. Three-dimensional thermal analysis of rectangular micro-scale inorganic light-emitting diodes integrated with human skin. *Int. J. Therm. Sci.* **2018**, *127*, 321–328. [CrossRef]
20. Zhang, J.P.; Li, Y.H.; Xing, Y.F.; Song, J.Z. Three-dimensional thermomechanical analysis of epidermal electronic devices on human skin. *Int. J. Solids Struct.* **2019**, *167*, 48–57. [CrossRef]
21. Yin, Y.F.; Li, M.; Yuan, W.; Chen, X.L.; Li, Y.H. A widely adaptable analytical method for thermal analysis of flexible electronics with complex heat source structures. *Proc. R. Soc. A* **2019**, *475*, 20190402. [CrossRef] [PubMed]
22. Li, Y.; Chen, J.; Xing, Y.; Song, J. Analytical investigations on the thermal properties of microscale inorganic lightemitting diodes on an orthotropic substrate. *AIP Adv.* **2017**, *7*, 035208. [CrossRef]
23. Wang, C.J.; Sim, K.; Chen, J.; Kim, H.; Rao, Z.Y.; Li, Y.H.; Chen, W.Q.; Song, J.Z.; Verduzco, R.; Yu, C.J. Soft ultrathin electronics innervated adaptive fully soft robots. *Adv. Mater.* **2018**, *30*, 1706695. [CrossRef] [PubMed]
24. Cui, Y.; Li, Y.H.; Xing, Y.F.; Ji, Q.G.; Song, J.Z. Thermal design of rectangular microscale inorganic light-emitting diodes. *Appl. Therm. Eng.* **2017**, *122*, 653–660. [CrossRef]
25. Wondu, E.; Lule, Z.; Kim, J. Thermal conductivity and mechanical properties of thermoplastic polyurethane-/silane-modified Al_2O_3 composite fabricated via melt compounding. *Polymers* **2018**, *11*, 1103. [CrossRef]
26. Li, R.; Li, Y.H.; Lu, C.F.; Song, J.Z.; Saeidpouraza, R.; Fang, B.; Zhong, Y.; Ferreira, P.M.; Rogers, J.A.; Huang, Y.G. Thermo-mechanical modeling of laser-driven non-contact transfer printing: Two-dimensional analysis. *Soft Matter* **2012**, *8*, 7122–7127. [CrossRef]